No significant steady-state surface creep along the North Anatolian fault offshore Istanbul: results of 6 months of seafloor acoustic ranging

P. Sakic[1], H. Piété[2], V. Ballu[1], J.-Y. Royer[2], H. Kopp[3], D. Lange[3], F. Petersen[3], S. Özeren[4], S. Ergintav[5], L. Geli[6], P. Henry[7] and A. Deschamps[2]†

[1] Laboratoire Littoral Environnement et Sociétés, CNRS and Université de La Rochelle, La Rochelle, France.
[2] University of Brest and CNRS, Laboratoire Géosciences Brest, IUEM, Plouzané, France.
[3] FB4 Dynamik des Ozeanbodens, GEOMAR Helmholtz-Zentrum für Ozeanforschung, Kiel, Germany.
[4] Eurasian Institute of Earth Sciences, Istanbul Teknik Üniversitesi, Istanbul,Turkey.
[5] Bogazici University , Kandilli Observatory and Earthquake Research Institute, Department of Geodesy, Cengelkoy-Istanbul, Turkey.
[6] Laboratoire Aléas géologiques et Dynamique sédimentaire, Ifremer, Plouzané, France.
[7] Systèmes & Réservoirs sédimentaires, Collège de France, Aix en Provence, France.
† Anne Deschamps passed away on December 26th 2014, as PI she played a major role in designing and conducting the experiment.
Corresponding author: Valérie Ballu (valerie.ballu@univ-lr.fr)

Contents of this file

Text S1
Tables T1 to T2
Figures F1 to F9

Introduction

The supporting information presents the inversion methodology and equations, the instruments configuration and design, the collected data and the results for the 6 first months of the seafloor geodesy experiment carried in the Marmara Sea, Turkey, across the Istanbul-Silivri segment :

- Presentation of the non-linear least-square inversion methodology and equations (Text S1)
- Characteristics of the deployed seafloor transponders (Table T1 and Figure F1)
- Time series of the different data collected by the transponders (Figures F2 to F7)
    - Baselines length evolution (Figure F2 to F5)
    - Water temperature recorded by each device (Figure F6)
- Tilt (pitch and roll) of each device (Figures F7)
- Results of the least-square processing, using different inversion parameters (Table T2 and Figure F8)
    - Baselines deformation rate φ
    - Sound-speed drift estimation κ
- Theoretical displacements expected for a simple fault model with various locking depths (F9).

Text S1

We present here the non-linear least-square inversion methodology and equations that we developed to process together data from the 10 transponders and associated temperature and pressure sensors. We designed our inversion to simultaneously determine the two sets of independent variables: sound-speed drift at each site and baseline-length variation between sites. Input observations are sound-speeds (derived from observed pressure and temperature) at each site, and acoustic travel-times between pairs of sites. The unknowns are solved with different hypotheses on the behavior of the baselines located on either side of the fault (fixed or constrained, presented in section S1.2.1 and S1.2.2, respectively) and on the sound-speed drift (section S1.2.3).

S1.1 Approach and formulation

Based on the elementary relation $\tau = \frac{d}{c}$ where τ is the one-way travel-time, c the sound-speed, and d the baseline-length between a transponder pair, the observation equation for each pair of transponders A and B can be written as follows:

$$\tau_{theo,i,A \to B} = \frac{1}{2} \left(d_{0,A \to B} + \varphi_{A \leftrightarrow B} t_i \right) \cdot \left(\frac{1}{c'_{A,i} + \kappa_A . t_i} + \frac{1}{c'_{B,i} + \kappa_B . t_i} \right)$$

with :

$\tau_{theo,i,A \to B}$ the theoretical one-way travel-time from transponder A to transponder B at epoch i,

$d_{0,A \to B}$ the baseline-length [m] between transponders A and B at the reference epoch,

$\varphi_{A \leftrightarrow B}$ the (constant) deformation rate of the baseline-length between transponders A and B [m/yr],

t_i the epoch [yr] of the ping relative to the reference,

κ_A, κ_B the coefficients of the sound-speed linear drift for transponder A and B respectively [m/s/yr],

$c'_{A,i}, c'_{B,i}$ the computed sound-speed [m/s] at transponders A and B at epoch i.

In our modeling, the observables are $\tau_{obs,i,A \to B}$, $c'_{A,i}$ and $c'_{B,i}$. For each logging session at epoch i, $\tau_{obs,i,A \to B}$ is the averaged time travel between transponders A and B and $c'_{A,i}$ and $c'_{B,i}$ the

averaged sound-speed derived from observed temperature and pressure respectively at sites A and B.

The estimated parameters are the n_{d_0} values of $d_{0,A \to B}$ (for n_{pair} transponder pairs, $n_{d_0} = 2n_{pair}$, because there might be a slight offset between $d_{0,A \to B}$ and the reciprocal $d_{0,B \to A}$), the n_φ values of $\varphi_{A \leftrightarrow B}$ ($n_\varphi = n_{pair}$), the n_κ values of κ_A and κ_B ($n_\kappa = n_{transponders}$).

We define the unknown vector X as

$$X = \left[d_{0,i_{d0}}, \varphi_{i_\varphi}, \kappa_{i_\kappa} \right]$$

with $i_{d0} \in [\![1, 2n_{pair}]\!]$, $i_\varphi \in [\![1, n_{pair}]\!]$, $i_\kappa \in [\![1, n_{transponders}]\!]$,

and the vector of theoretical travel-times as:

$$T_{theo} = \left[\tau_{theo,i_\tau} \right]$$

with $i_\tau \in [\![1, n_{pings}]\!]$.

We define the function f such as:

$$f : X \to T_{theo}(X)$$

To linearize the problem, we define the design matrix A, i.e. the matrix of partial derivatives of each theoretical observation with respect to the unknowns.

$$A = \frac{\mathrm{d}f}{\mathrm{d}X} = \begin{bmatrix} \dfrac{\mathrm{d}\tau_{theo,1}}{\mathrm{d}d_{0,i_{d0}}} & \cdots & \dfrac{\mathrm{d}\tau_{theo,1}}{\mathrm{d}\varphi_{i_\varphi}} & \cdots & \dfrac{\mathrm{d}\tau_{theo,1}}{\mathrm{d}\kappa_{i_\kappa}} \\ \vdots & & \ddots & & \vdots \\ \dfrac{\mathrm{d}\tau_{theo,n_{pings}}}{\mathrm{d}d_{0,i_{d0}}} & \cdots & \dfrac{\mathrm{d}\tau_{theo,n_{pings}}}{\mathrm{d}\varphi_{i_\varphi}} & \cdots & \dfrac{\mathrm{d}\tau_{theo,n_{pings}}}{\mathrm{d}\kappa_{i_\kappa}} \end{bmatrix}$$

If B is the vector of the difference between the observed travel-times and the predicted values, ($B = T_{obs} - T_{theo} = \left[\tau_{obs,i} - \tau_{theo,i_\tau} \right]$), the problem is a standard least-square problem which can be written as follows:

$$B = A\delta X + V$$

with δX the correction values to X so that the unknown X respect the least-square condition and V, the vector of residuals.

The objective is to minimize the difference between the observed travel-times and the predicted ones in a least-square sense (i.e. to minimize the sum of the squared residuals $\sum V^T V$). The least-square model (e.g. *Strang and Borre, 1997*) allows the definition of the so-called "normal equation" :

$$A^T A \delta \hat{X} = A^T B$$

$$\delta \hat{X} = (A^T A)^{-1} A^T B$$

The new estimated values are $X_{new} = X + \delta \hat{X}$, and the problem is solved iteratively; the solution is usually obtained after 3 iterations, using $\sum \delta \hat{X} < \omega$ as a stop criteria, where ω is a quasi-null arbitrary value of 10^{-10}.

S1.2 Application of constraints

In the inversion, changes in baselines are treated in three different ways: they are either let entirely unconstrained ("free mode") or set to a given value, for instance zero, ("fixed mode") or constrained to tend towards a given value, with a chosen uncertainty or weight ("constrained mode"). These conditions are differently applied whether the baseline crosses or does not cross the fault, since we assume that all the strain occurs along the fault.

S1.2.1 Fixing baselines on either side of the fault

To impose null values on the φ parameter for baselines that do not cross the fault, we use the Helmert's method described by *Ghilani (2011)*. If we have n_{Fix} fixed baselines, the normal equation is augmented by the constraint equations as follows:

$$\begin{bmatrix} A^T A & F^T \\ F & 0 \end{bmatrix} \begin{bmatrix} \delta X \\ \Lambda \end{bmatrix} = \begin{bmatrix} A^T B \\ B_{Fix} \end{bmatrix}$$

B_{Fix} is the vector of the constrained values, which can be written:

$$B_{Fix} = \left[\varphi_{Fix,i_{Fix}} \right]_{n_{Fix}}$$

So, in our case:

$$B_{Fix} = [0]_{n_{Fix}}$$

F   is the binary matrix of the constraint equations, where $F_{i,j} = 1$ when $\delta X_j = B_{Fix,i}$ is required, and 0 elsewhere,

Λ is the vector of Lagrangian multipliers.

S1.2.2 Constraining baselines towards specific values

Another way to control the baseline behavior is to constrain the φ parameter to a given value with an uncertainty set by weights on the parameter (*Strang and Borre, 1997*). The approach is to treat the φ parameters as observables, alongside with the travel-times and thus to set an additional observation equation for each baseline we wish to constrain:

$$g: \varphi_{A\leftrightarrow B} \longrightarrow \phi_{Constr,A\leftrightarrow B}$$

The observation vector T_{Theo} has a new component $\phi_{Constr,A\leftrightarrow B}$, and the matrix A an additional partial derivative $\frac{dg}{dX}$.

For this approach, a weight matrix P must be introduced, to normalize the two observables τ and ϕ of different nature, respectively with weights p_τ and p_ϕ. The weight p_i of an observable i is defined as $\frac{1}{\sigma_i^2}$ where σ_i is the standard deviation of the observable i.

$$P = diag\left(\underbrace{p_\tau, \quad \cdots \quad ,p_\tau}_{n_\tau} \underbrace{p_\phi, \quad \cdots \quad ,p_\phi}_{n_\phi}\right)$$

To account for the weighting, the normal equation becomes:

$$\delta\hat{X} = (A^T P A)^{-1} A^T P B$$

Based on travel-time short-term repeatability, the weights for the travel-time observations are taken as $\sigma_\tau = 2\mu s$. The weights on the φ parameters depend on how strongly we want to constrain them to the targeted value (which, in our case, is 0 on either side of the fault). We tested $\sigma_\phi = 10^{-2}$, 10^{-4} and 10^{-6} mm/yr; the latter value yields similar results to the fixed baseline case described above. A single φ parameter is estimated for common baselines in the F and G networks.

S1.2.3 Constraining sound-speed drift

To avoid excessive and, thus, unrealistic values in sensor drift parameters, we imposed κ coefficients to tend towards zero with a σ_κ standard deviation, using a method similar to the one described above. σ_κ is determined from the manufacturer's sensor drift uncertainties, 9 ppm/yr and 7 ppm/yr, respectively for the temperature and pressure sensors, which gives $\sigma_\kappa = 2.6 \times 10^{-5}$ m/s/yr on the resulting sound-speed drift.

	Network F	Network G
	University of Brest	Geomar Institute
Acoustic stations		
Number of stations	4	6
Acoustic transponder	Sonardyne AMT (22.5 kHz)	Sonardyne AMT (17.0 kHz)
Temperature sensor	Valeport	Sonardyne
Pressure sensor	Paroscientific Digiquartz	Paroscientific Digiquartz
Sound-speed sensor	Valeport	Valeport
Inclinometer sensors	Jewell	Jewell
Session parameters		
Session interval	1h	2h
Wake-up interval as Master	5 min	20 min
Number of samples / session		
Ranges	3 at 5s interval	1
Sound-speed	10 (1 as Master + 3*3 as Slave)	2 (1 as Master + 1 as Slave)
Temperature	10 (1 as Master + 3*3 as Slave)	2 (1 as Master + 1 as Slave)
Pressure	1	1
Attitude (on orthogonal axes)	1 every 24h (24 sessions)	1 every 20h (10 sessions)
Number of ranging per baseline		
Per session	6	2
Per day	144	24
Expected autonomy	5 years	3 years

Table T1. Configuration and logging sessions of the acoustic transponders in Geomar (G) and University of Brest (F) subsea geodetic networks deployed in the Kumburgaz Basin.

κ [m/s/yr]							
Station number	Fig. 2	Fig. H.a)	Fig. H.b)	Fig. H.c)	Fig. H.d)	Fig. H.e)	Fig. H.f)
Sound-speed drift	Constrained	Free	Constrained	Free	Constrained	Free	Constrained
2304 & 2001	6.75E-05	3.71E-02	3.75E-05	-3.55E-04	3.25E-05	-2.84E-04	2.20E-07
2305 & 2002	-1.77E-05	-1.77E-02	-2.72E-05	-1.66E-02	-2.46E-05	-1.66E-02	-4.00E-08
2302 & 2004	4.38E-05	1.87E-02	3.91E-05	5.41E-02	3.40E-05	5.41E-02	9.00E-08
2307 & 2003	-8.91E-06	2.37E-03	-3.07E-05	-5.85E-03	-2.83E-05	-5.86E-03	-1.50E-07
2303	-1.74E-05	-2.16E-02	-2.30E-05	-2.17E-02	-2.23E-05	-2.17E-02	-8.00E-08
2301	-2.17E-06	1.98E-03	-4.36E-06	-6.97E-02	-4.16E-06	-6.97E-02	-1.00E-08

Table T2A. Estimated sound-speed drift κ corresponding to the least-square inversions presented in figures 2 and F8. Constrained models use $\sigma_\kappa = 2.6 \times 10^{-5}$ m/s/yr . SV = Sound-Velocity.

φ [mm/yr]							
	Fig. 2	Fig. H.a)	Fig. H.b)	Fig. H.c)	Fig. H.d)	Fig. H.e)	Fig. H.f)
Baselines on either side of the fault	Fixed	Fixed	Fixed	Fixed	Constrained $\sigma = 10^{-4}$m/yr	Constrained $\sigma = 10^{-4}$m/yr	Constrained $\sigma = 10^{-4}$m/yr
2301-2302	0	0	0	0	1.1E-01	-6.2E-03	2.4
2301-2304	0	0	0	0	3.8E-01	8.9E-03	8.1
2302-2304 & 2001-2004	0	0	0	0	-1.9	7.1E-03	-14.8
2303-2305	0	0	0	0	4.9E-01	1.8E-03	10.8
2303-2307	0	0	0	0	3.4E-01	-8.7E-04	15.5
2305-2307 & 2002-2003	0	0	0	0	7.9E-01	-2.1E-03	6.4
Fault-crossing baselines	Constrained $\sigma = 10^{-4}$m/yr	Constrained $\sigma = 10^{-4}$m/yr	Constrained $\sigma = 10^{-4}$m/yr	Constrained $\sigma = 10^{-4}$m/yr	Free	Free	Free
2301-2303	11.9	11.6	10.2	-19.2	10.2	-19.2	10.2
2301-2305	-3.4	-3.5	-1.7	-12.0	-1.7	-12.0	-1.7
2301-2307	9.5	9.5	8.3	-13.7	8.3	-13.7	8.3
2302-2303	5.9	5.9	7.1	12.3	7.1	12.3	7.1
2302-2305 & 2002-2004	-3.0	-2.9	-6.1	0.1	-6.1	0.1	-6.1
2303-2304	9.2	9.5	5.8	-3.4	5.8	-3.4	5.8
2304-2305 & 2001-2002	3.1	3.6	0.3	-2.5	0.3	-2.5	0.3
2304-2307 & 2001-2003	12.9	13.8	1.3	0.2	1.3	0.2	1.3

Table T2B. Estimated lengthening/shortening rate φ corresponding to the least-square inversions presented in figures 2 and F8.
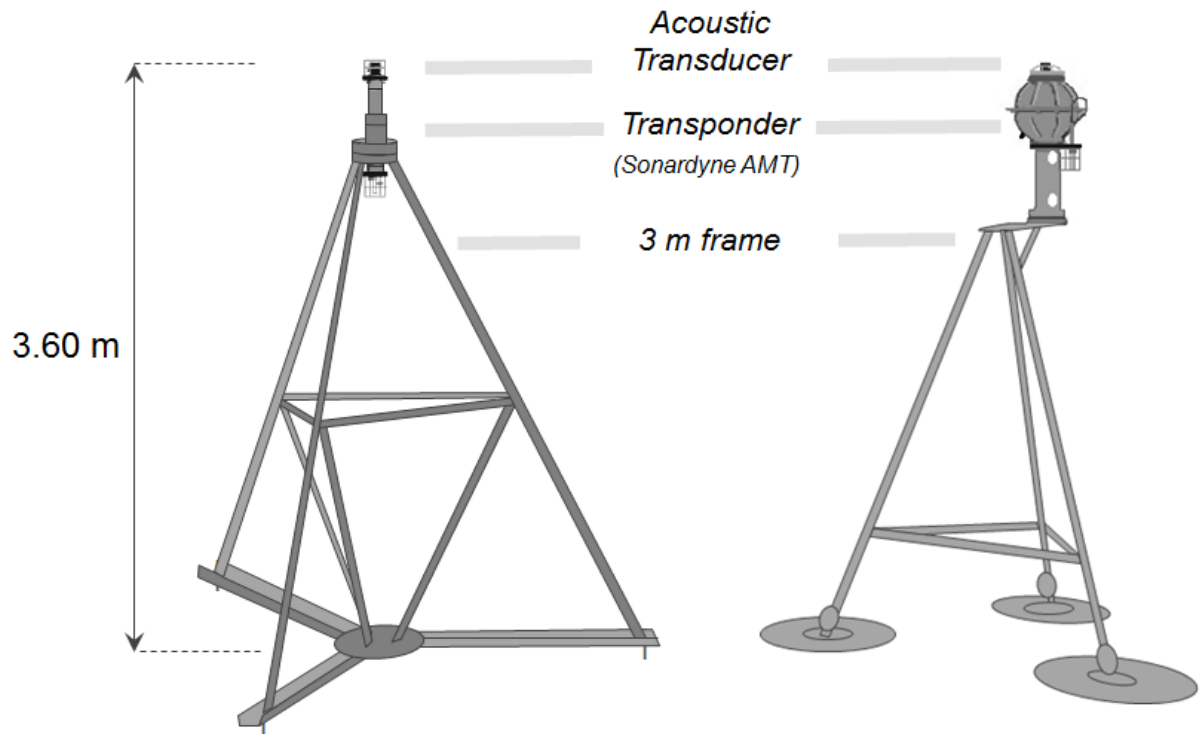
Figure F1. Seafloor acoustic ranging systems deployed in the Kumburgaz Basin in the Marmara Sea. Left, Geomar units (G network), right, University of Brest units (F network).
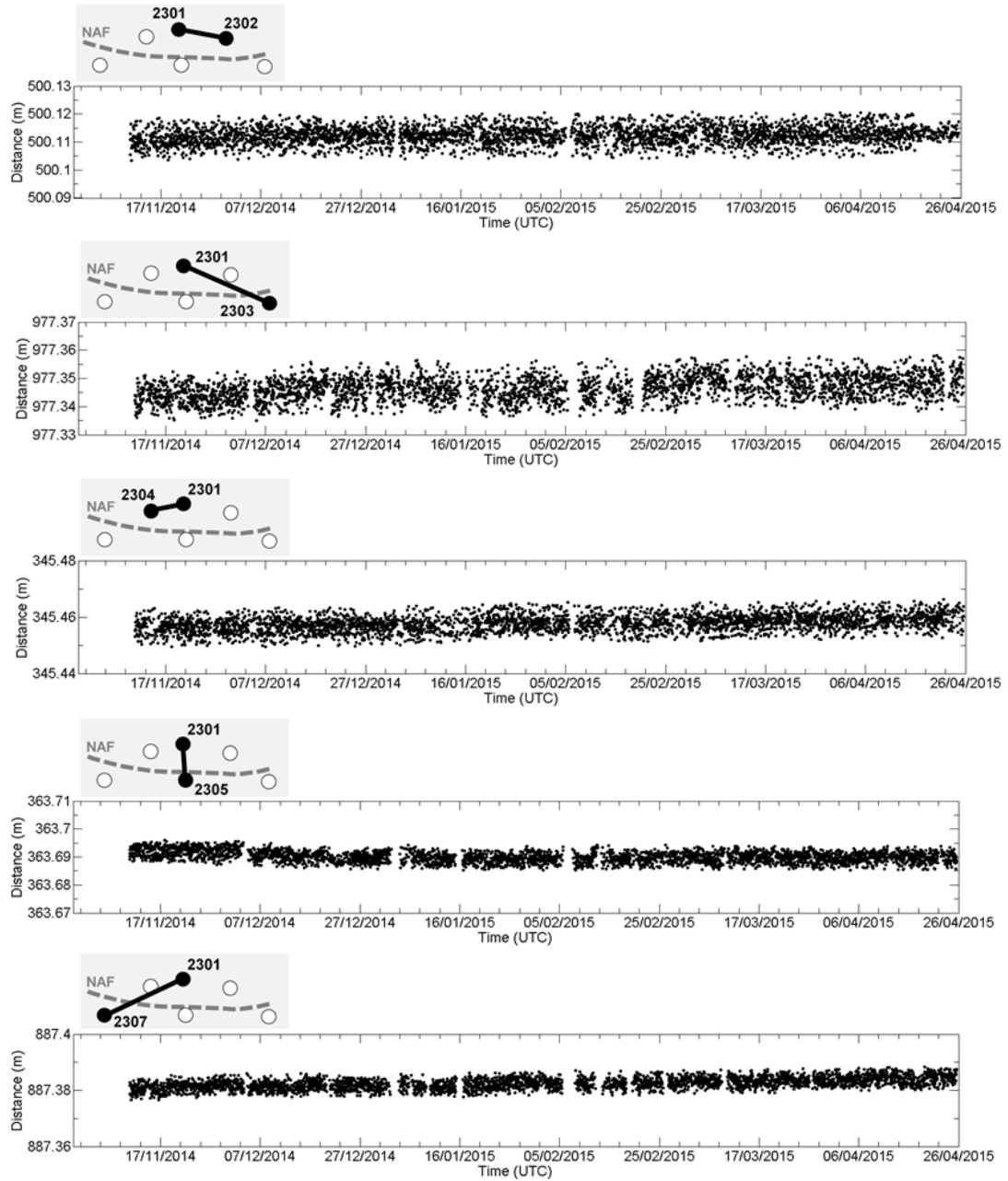
Figure F2. Distance time series derived from measurements along baselines of the G network. Circles in insets denote the position of the transponders.
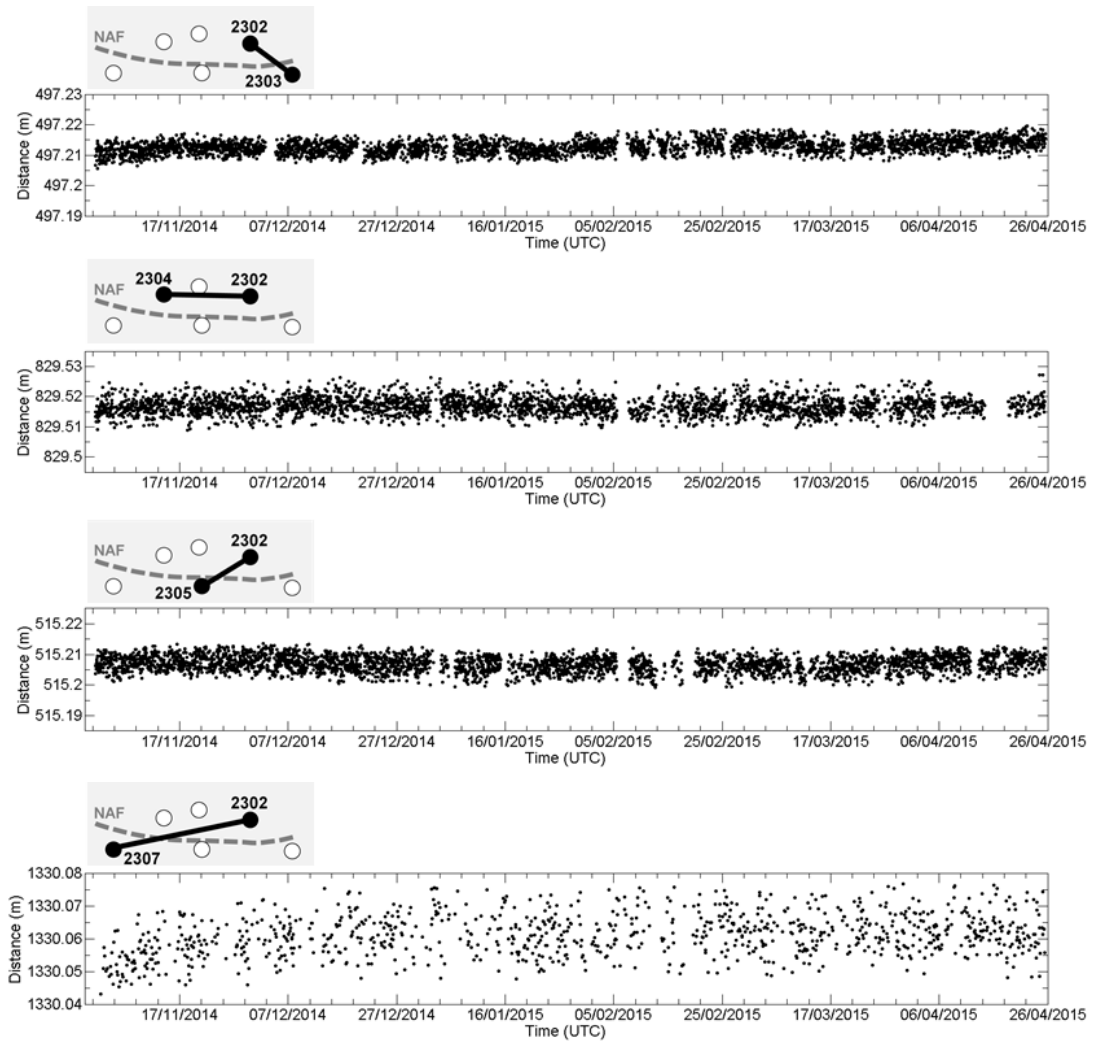
Figure F3. Distance time series derived from measurements along baselines of the G network. Circles denote the position of the transponders.
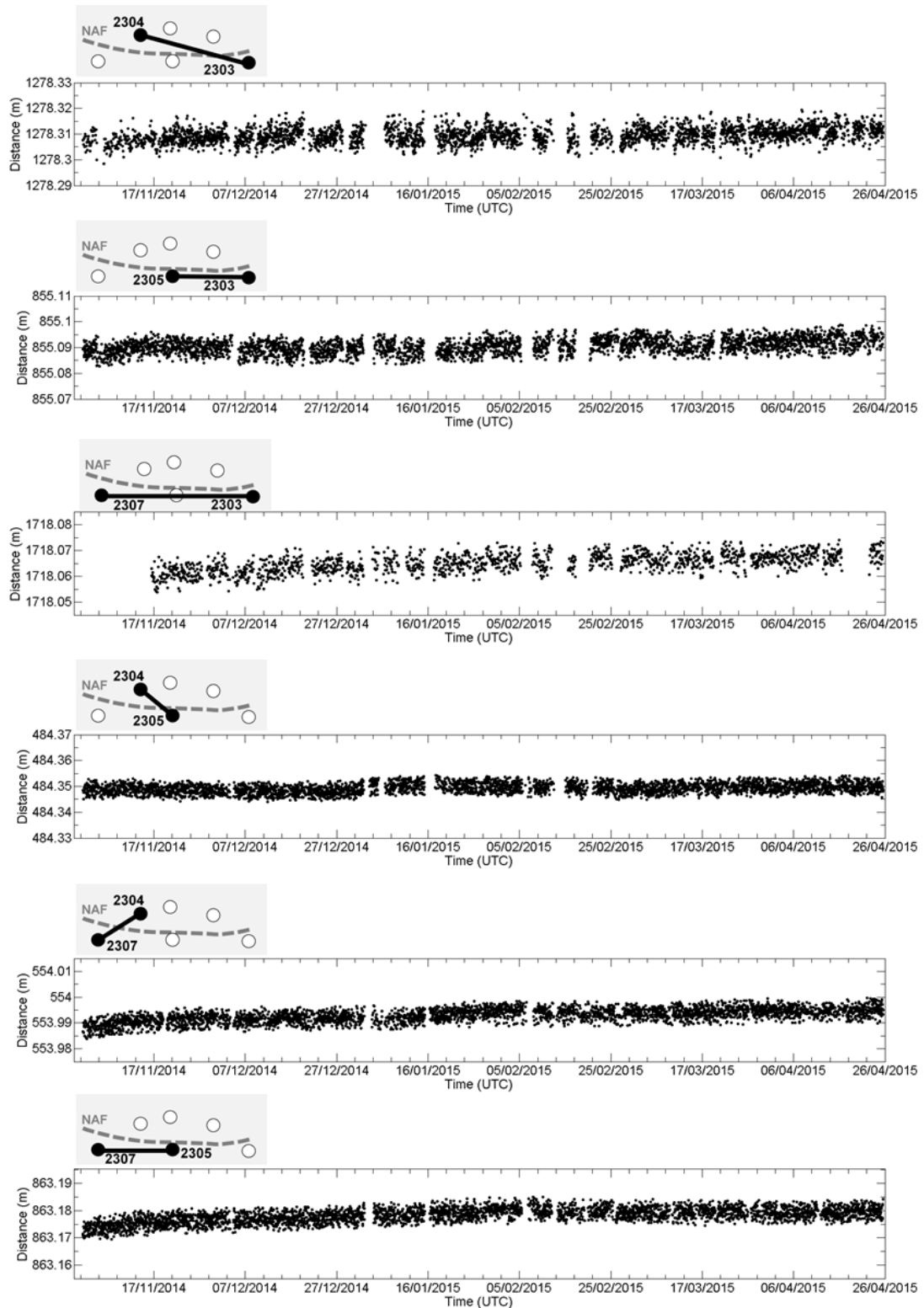
Figure F4. Distance time series derived from measurements along baselines of the G network. Circles denote the position of the transponders.
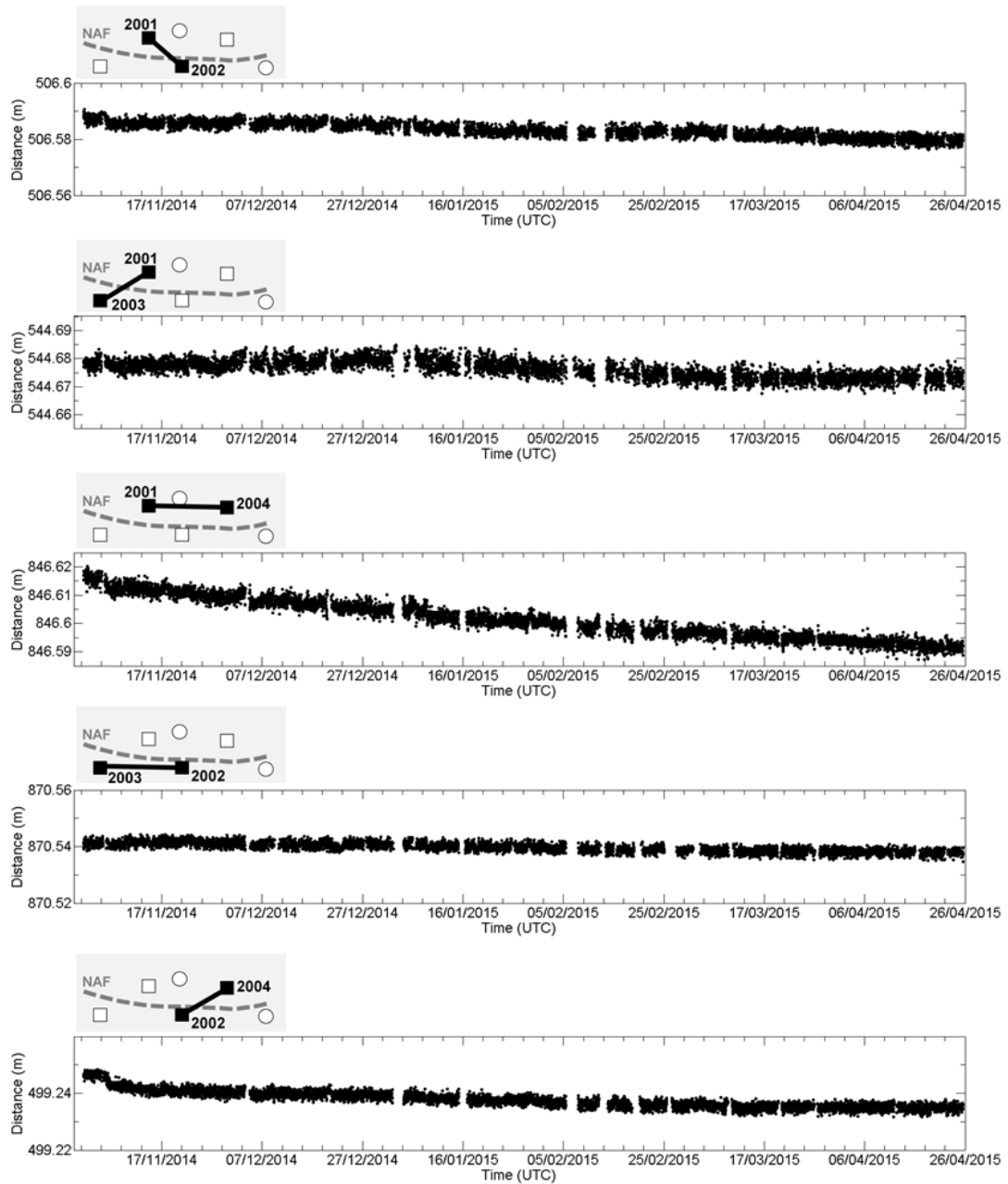
Figure F5. Edited distance time-series derived from measurements along baselines of the F network. Squares denote the position of the F transponders. Circles indicate the location of G transponders that are not collocated with the F units.
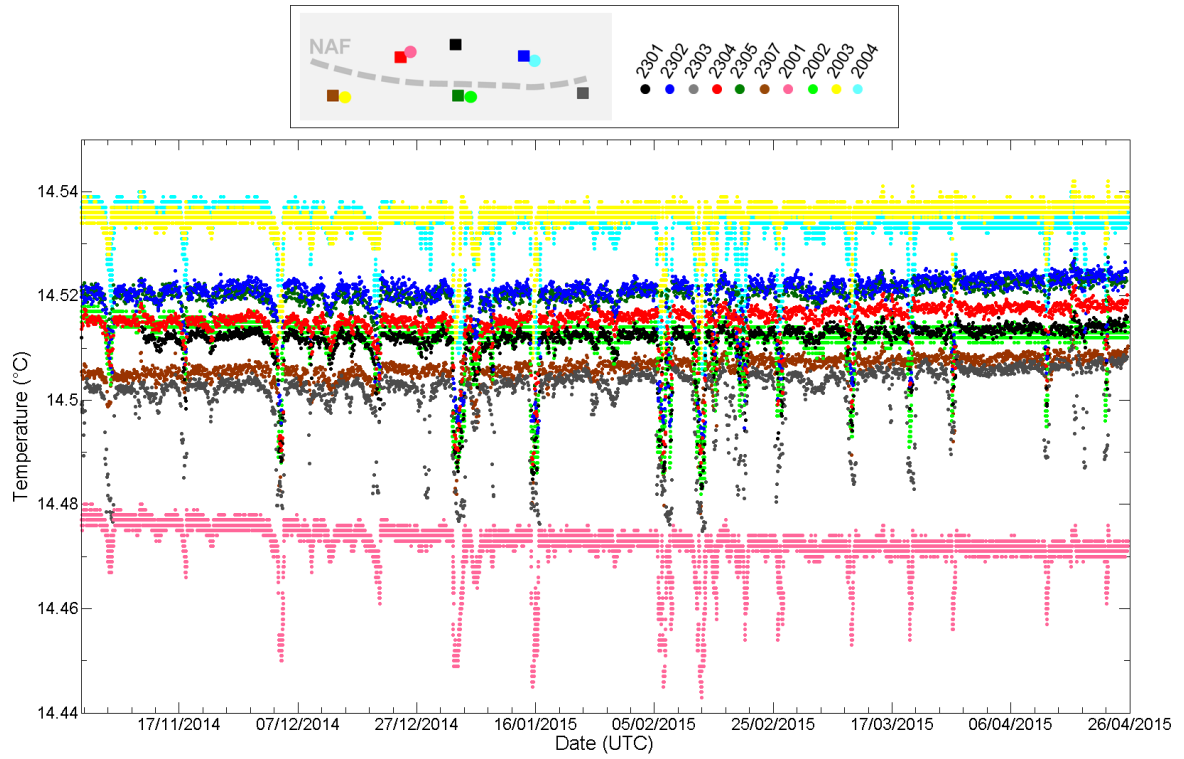
Figure F6. Temperature recorded by the transponders deployed in the Kumburgaz Basin. Logs evidence recurrent cold water pulses across the Kumburgaz Basin and linear trends in opposite direction for nearby sensors that we interpret as instrumental drifts.
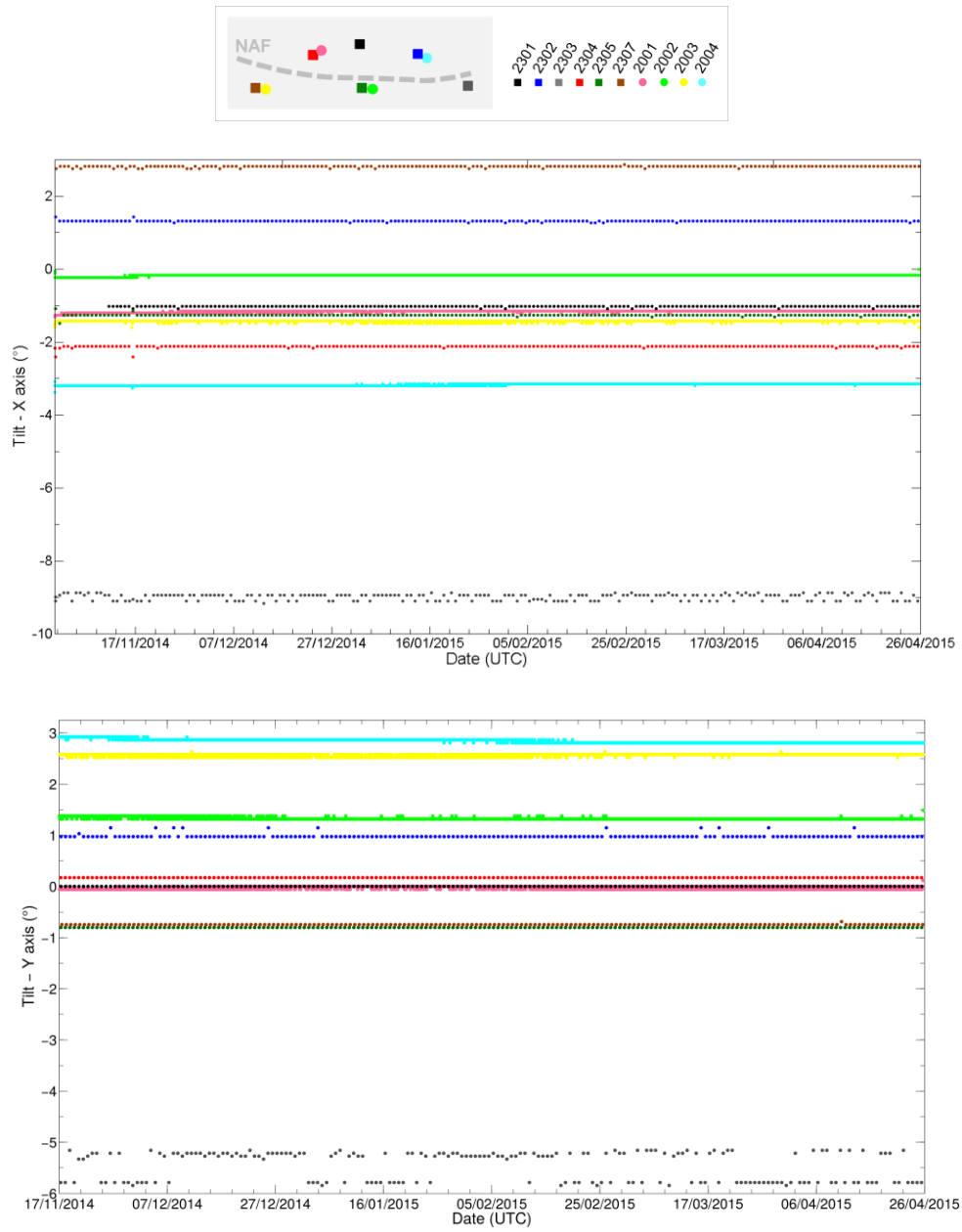
Figure F7. Tilt data recorded by orthogonal inclinometers of the transponders deployed in the Kumburgaz Basin. Only units F-2004 (cyan) and G-2303 (grey) display changes or oscillations in their attitude.
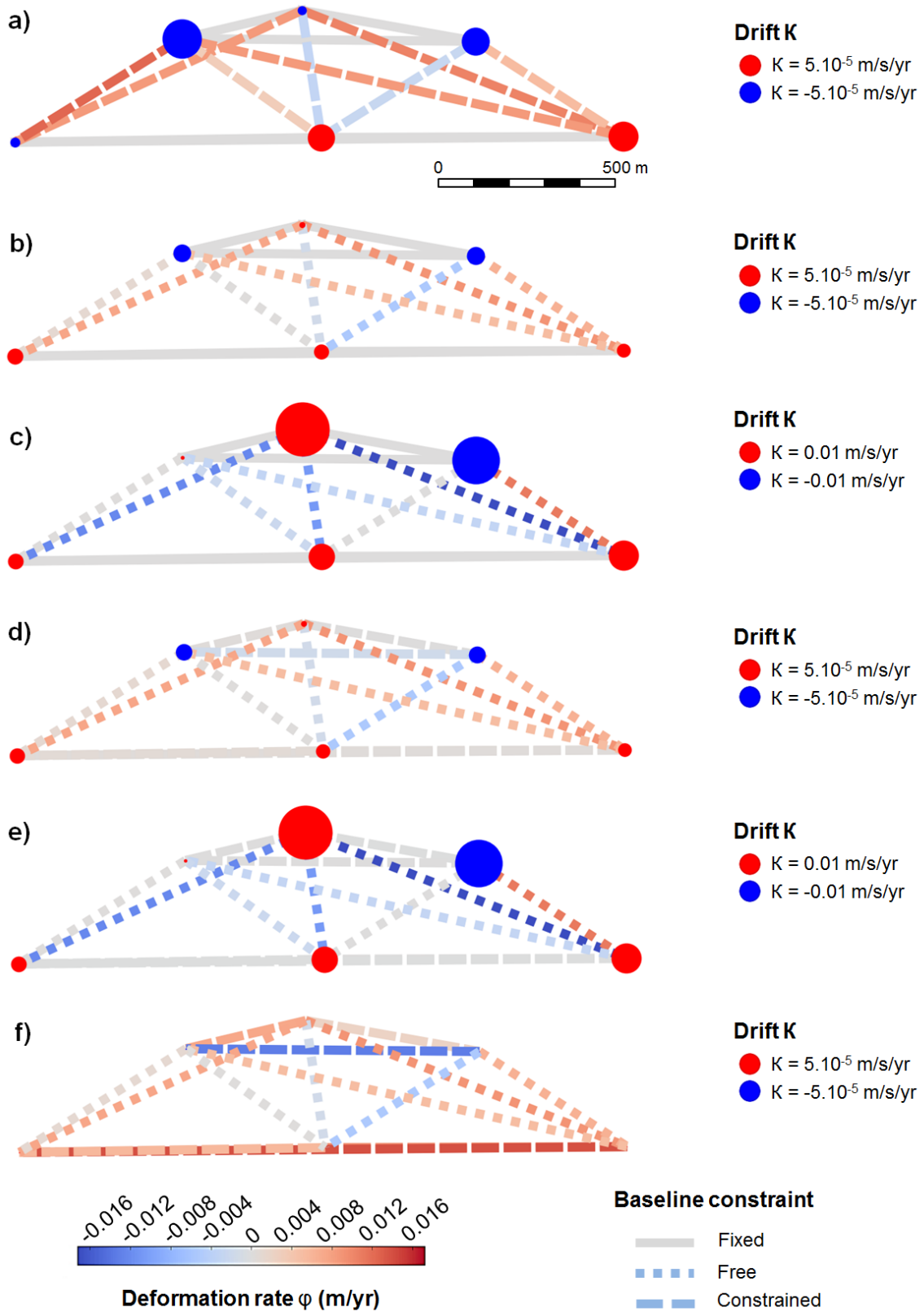
Figure F8. Results from least-square inversions of baseline data and sound-speed drifts,

16

assuming fixed (experiments a) b) c)) or constrained (experiments e) f) g)) baselines on either side of the fault, and for different conditions imposed on sound-speed drift (κ) and deformation rate (φ): a) free κ and constrained φ for fault-crossing baselines; b) constrained κ and free φ for fault-crossing baselines; c) free κ and φ for fault-crossing baselines; d) free φ for fault-crossing baselines, constrained φ for baselines on either side of the fault at 10^{-4} m/yr, free κ; e) free φ for fault-crossing baselines, constrained φ for baselines on either side of the fault at 10^{-4} m/yr, constrained κ f) free φ for fault-crossing baselines, constrained φ for baselines on either side of the fault at 10^{-2} m/yr, constrained κ. Deforming baselines are denoted by dashed lines, with color indicating the magnitude and sign of baseline-length variation. Estimated sound-speed drift is represented by circles of size proportional to its magnitude.
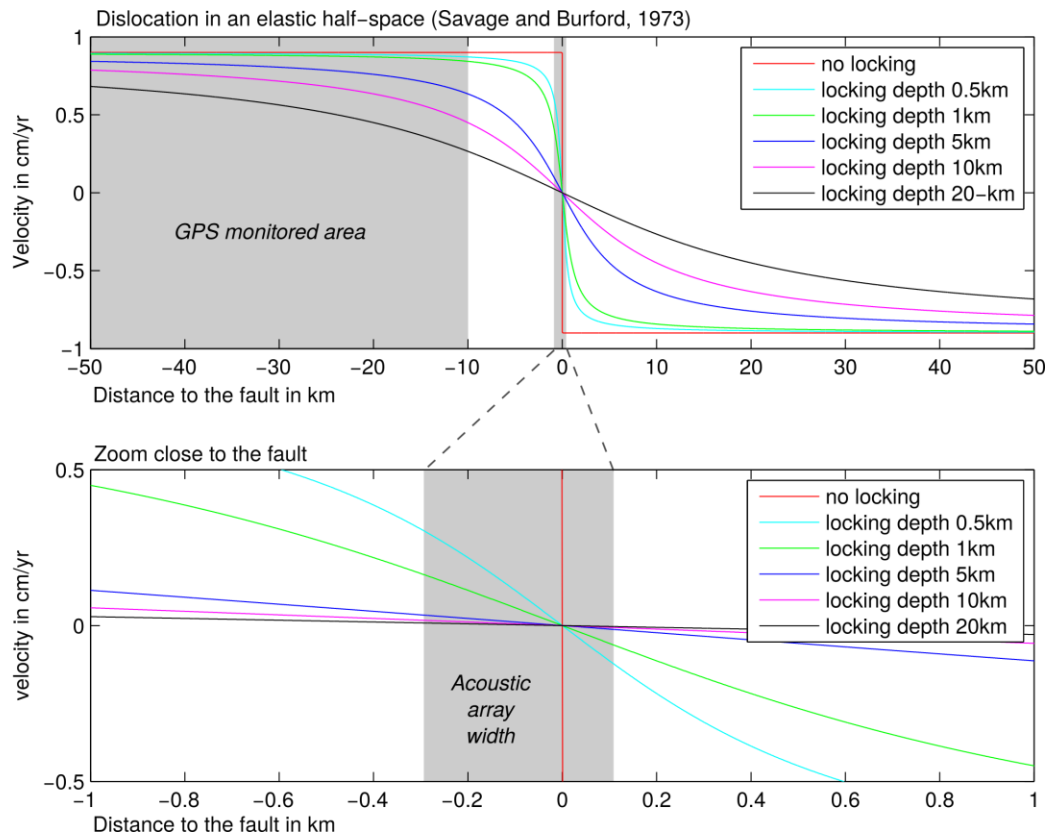
Figure F9: Theoretical displacements expected for a simple fault model with various locking depths. The displacements are computed using Savage and Burford (*1973*) formulation on a profile perpendicular to a vertical fault passing through our sub-marine geodetic network, assuming a 18 mm/yr far-field strike-slip motion. The grey shading shows areas monitored by on-land GPS stations and sub-marine acoustic ranging (this study). Although on-land GPS data could theoretically be sufficient to discriminate between various locking depths, available stations (*Ergintav et al. 2014*) are not well aligned relative to this profile and do not fully constrain any solution.

References

Savage, J.C. & Burford, R.O., 1973. Geodetic determination of relative plate motion in central California, *J. Geophys. Res.,* 78**,** 832-845.

Ergintav, S., Reilinger, R. E., Cakmak, R., Floyd, M., Cakir, Z., Dogan, U., King, R. W., McClusky, S., and H. Ozener (2014). "Istanbul's Earthquake Hot Spots: Geodetic Constraints on Strain Accumulation along Faults in the Marmara Seismic Gap." *Geophys. Res. Lett.* 41 (16): 5783–88. doi:10.1002/2014GL060985.